calculated at $f = 37$ GHz (Fig. 1). As the sphere radius is enlarged, the reflection first drops; at a critical radius $R_c = 1.02$ mm the reflection vanishes, and for larger radii it grows back. The sensitivity to radius R is small, and any value between 0.96 and 1.10 mm results in reflection lower than –30 dB.

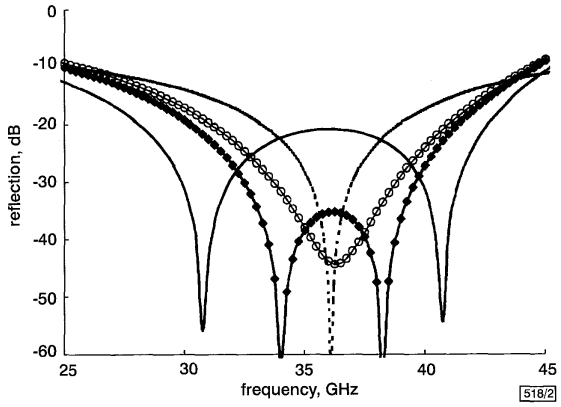

Fig. 2 *Reflection coefficient of normally incident plane-wave from metal-dielectric windows ($d = 4$ mm, $\varepsilon_r = 2.2$, $a = 4$ mm) with different sphere radii, and from dielectric slab ($d = 2.67$ mm, $\varepsilon_r = 2.2$)*

——— $R = 0.88$ mm
—◆— $R = 1.00$ mm
—○— $R = 1.04$ mm
– – – – dielectric slab

To better understand the performance of this metal-dielectric window, the reflection coefficient of several windows with different radii R against frequency is shown (Fig. 2). The original $d = \lambda/2$ and $d = \lambda$ zeros of the non-loaded dielectric window migrate toward one another as R approaches R_c, and at the same time the reflection level at the centre frequency drops. This is typical of a double-zero system. At $R = R_c$ the two zeros coalesce, and for larger radii the two zeros move into the complex frequency plane, and the frequency response shows a shallow single dip. In practice, the acceptable reflection level at the central frequency is decided, which then dictates the value of R ($R < R_c$).

Obviously, the new window has a frequency bandwidth larger than that of the half-wavelength window. To demonstrate this, the reflection coefficient of a pure dielectric window 2.67 mm thick is added, having its first transmission resonance at the same central frequency (Fig. 2).

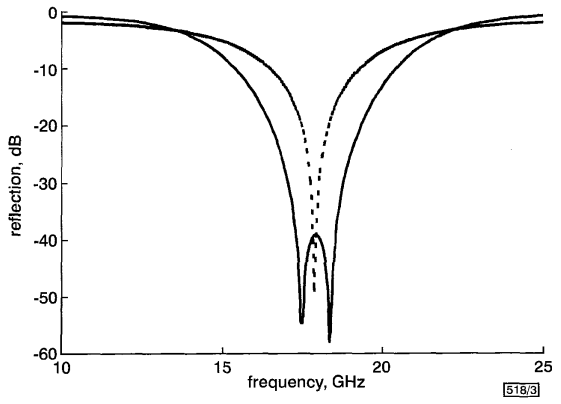

Fig. 3 *Reflection coefficient of normally incident plane-wave from metal-dielectric window and dielectric slab*

——— metal-dielectric window ($d = 4$ mm, $\varepsilon_r = 9.2$, $a = 2$ mm, $R = 0.87$ mm)
– – – – dielectric slab ($d = 2.67$ mm, $\varepsilon_r = 9.2$)

Although the example above used a low dielectric-constant material, similar designs can handle high dielectric-constant materials also. Fig. 3 shows the reflection coefficient of a normally incident plane-wave at a window with the following parameters; $d = 2.0$ mm, $\varepsilon_r = 9.2$, $a = 4.0$ mm and $R = 0.87$ mm. It has the same typical double-zero response with a narrower bandwidth.

Conclusions: The design of a new type of a thick metal-dielectric window that gives a frequency bandwidth three times wider than a simple half-wavelength window has been demonstrated. Other aspects of the design, such as oblique incidence, different inclusions (boxes, cylinders), and multi-layer designs will be discussed in future publications.

13 September 2001
Electronics Letters Online No: 20010958
DOI: 10.1049/el:20010958

A. Frenkel (*Anafa - Electromagnetic Solutions Ltd., Haganim St. 1, Kiriat Bialik, P.O.B 5301, Israel 27000*)

E-mail: avri@anafa-em.com

References

1 WALTON, J.D., Jr. (Ed.): 'Radome engineering handbook: design and principles' (Marcel Dekker, New York, 1970)
2 KOZAKOFF, D.J.: 'Analysis of radome-enclosed antennas' (Artech House, 1997)
3 MUNK, B.A.: 'Frequency selective surfaces – theory and design' (John Wiley & Sons Inc., 2000)
4 CHUPRIN, A.D., PARKER, E.A., and BATCHELOR, J.C.: 'Resonant frequencies of open and closed loop FSS arrays', *Electron. Lett.*, 2000, **361**, (19), pp. 1601–1603
5 SHAVIT, R., SMOLSKI, A.P., MICHIELSSEN, E., and MITTRA, R.: 'Scattering analysis of high performance large sandwich radomes', *IEEE Trans. Antennas Propag.*, 1992, **40**, pp. 126–133
6 VIDAL, P.F. and GOODRICH, F.N.S.: United States Patent No. 4,467,330, 'Dielectric structures for radomes', August 21, 1984
7 FRENKEL, A.: GB patent application No. 0120075.7, 'Electromagnetic window', August 17, 2001

Atrial defibrillation using low tilt pulses delivered by transcutaneous RF coupling

J.A. Santos, G. Manoharan, N.E. Evans, J.McC. Anderson, B.J. Kidawi, J.D. Allen and A.A.J. Adgey

A new form of atrial defibrillator is described, employing a transdermal transformer to couple a 7.2 MHz RF pulse to an implanted, passive receiver; this, in turn, delivers a low-tilt unipolar DC shock to the heart. In animal studies, cardioversion was 100% successful with pulses of 100 V amplitude and 10 ms width.

Introduction: Fibrillation is a chaotic electric excitation of the myocardium and results in a loss of the coordinated mechanical contraction of a normal heartbeat. Atrial fibrillation (AF) is the most common arrhythmia, characterised by irregular and chaotic fibrillatory waves, giving rise to a loss in the normal P wave that normally precedes the QRS complex of an electrocardiogram (ECG) [1]. Cardioversion to sinus rhythm has traditionally been attempted by pharmacological measures or transthoracic direct current shock. These have varying success rates, risks and cost implications. Although atrial arrhythmias are not usually dangerous, they may precipitate heart failure if the rate is very rapid or if there is underlying valvular, myocardial or coronary disease [2]. To enhance the treatment process, there has been interest in catheter-based transvenous atrial defibrillation and its potential use in an implantable atrial defibrillator [3]. Implantable defibrillators are traditionally complex devices requiring on-board pattern recognition with extensive recording and follow-up procedures. The nature of AF may not require the sophistication associated with such automatic recognition and delivery techniques. Accordingly, a new approach has been initiated which involves the implantation of essentially passive circuitry only, powered via the transdermal delivery of radio frequency (RF) energy. In the demonstration phase achieved to date, animal cardioversion has been effected using external control.

Method: The defibrillator system, shown in Fig. 1, consists of an on-off pulsed power source operating at 7.2 MHz and connected

to a custom-built RF transformer; the latter is built with a series-tuned primary placed on the body surface and a parallel-tuned, intracorporeal secondary acting as the 'receiver'. This configuration maximises the coupling properties of each side of the circuit when resonance is achieved at the desired frequency [4]. Using a drive frequency of 7.2 MHz gives physically viable inductance values and avoids excessive detuning by stray body capacitance. The axial coupling distance of the transformer, D, was set at 22 mm and the secondary coil diameter, d_s, restricted to 35 mm to ensure clinical acceptability. The optimum primary coil diameter, d_p = 53 mm, was calculated from [5]:

$$d_p^2 = d_s^2 + 4D^2 \quad (1)$$

The final inductance of the primary winding was 10 μH, series-tuned to resonance at 7.2 MHz with a 47 pF high voltage pulse capacitor. The 5.9 μH secondary inductor was parallel-tuned by a capacitive matching network to the (nominal) 50 Ω resistive load presented by the heart. Measurements gave the maximum mutual inductance as 150 nH, with a coupling coefficient k = 0.02. A triple Schottky-diode-stack was used as a half-wave rectifier to generate the unipolar stimulus. This was delivered transvenously to the heart via two defibrillation leads, one placed in the distal coronary sinus and the other in the right atrial appendage. Fig. 2 shows the final waveform obtained, alongside that normally generated by capacitor discharge systems; the low voltage tilt on-load enables a higher overall energy to be delivered in a given defibrillating pulsewidth.

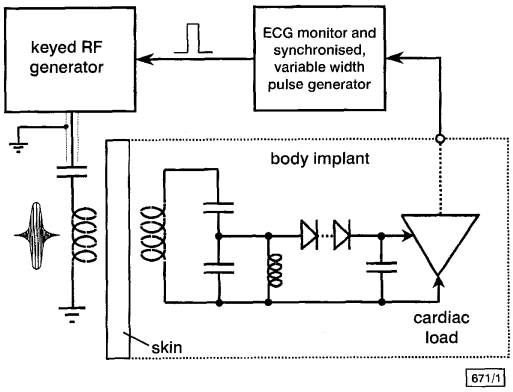

Fig. 1 *RF-coupled implantable atrial defibrillator system*

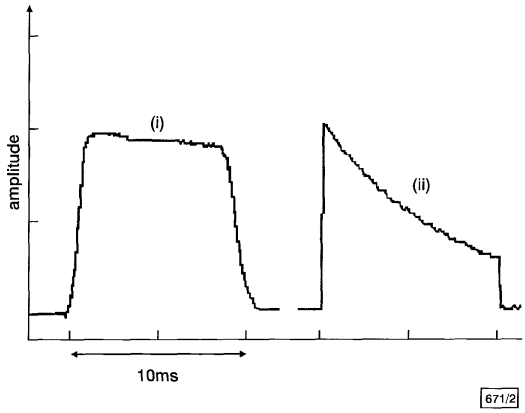

Fig. 2 *Comparison of low-tilt pulse achieved in RF pulse defibrillation with wave shape typically found in switched capacitor defibrillators*

(i) transdermal RF pulse defibrillator
(ii) switched capacitor defibrillator

The device was tested using 10 anaesthetised sheep. Sustained AF was induced by rapid atrial pacing (Grass stimulator, 100 Hz, 5 V) and defibrillation was attempted, synchronised to the QRS complex. The efficacy of three different rectified DC pulse amplitudes (50, 75 and 100 V) was assessed using keying pulsewidths in the range 5–30 ms. Pulse rise and fall times were 200 μs and 1.2 ms, respectively. Defibrillation was repeated 5 times at each voltage and pulsewidth setting. AF was re-induced if cardioversion was successful. All shock voltage and current waveforms were captured for later analysis: this enabled Joule delivery levels to be calculated.

Table 1: Cardioversion success rate for different pulsewidths and amplitudes

Pulsewidth [ms]	% success rate at peak pulse amplitude		
	50 V	75 V	100 V
5	18	–	58
6	40	–	72
8	48	52	88
10	50	58	100
12	56	66	98
15	64	66	98
20	74	78	96
30	74	–	98

Table 2: Measured energy (J) delivered to cardiac load

Pulse amplitude	Pulsewidth			
	8 ms	12 ms	15 ms	20 ms
50 V	0.37	0.43	0.53	0.66
75 V	0.65	0.89	1.11	1.38
100 V	1.22	1.54	1.93	2.36

Results: As shown in Table 1, at 50 V the rate of successful conversion was only 40% for the smaller pulsewidths; this increased to 74% at 30 ms. Success rates were comparable at 75 V. At 100 V, however, 100% success was observed for 10 ms pulses: this figure fell to 98% when using 12 and 15 ms widths. The system proved resistant to lateral and angular coil misalignment, while maintaining high power transfer efficiency. At axial deviations of ±5 mm around maximum transfer the losses were less than 1 dB, indicating an acceptable displacement insensitivity. The lateral displacement characteristic was broader, with the measured loss reaching only 0.38 dB when displacing 10 mm below ideal alignment and 20 mm above it (the asymmetry was due to coupling between the power feed cable and the primary inductor). Table 2 shows the measured energy delivered to the body using the implant. Note that more energy delivered does not mean more chance of success. A trade-off has to be established between the duration of the pulse and the voltage supplied to accomplish defibrillation.

Conclusions: During the experiments no arrhythmic or haemodynamic complications were observed. Complete success was obtained using pulses of 100 V amplitude and 10 ms width, with a measured 1.54 J of delivered energy, indicating that this novel method is both feasible and safe in the cardioversion of AF. The absence of a battery makes the device attractive in terms of minimising potential hazard and thus provides an inexpensive and viable alternative method of treatment for patients suffering paroxysmal AF. Future work will include the realisation of a bipolar-pulse delivery system to minimise pain during treatment and the implementation of auto-tuning using return-path telemetry to monitor the transmission of energy to the implant.

Acknowledgments: This work has received financial support from the ALFA-BETA Programme, the University of Ulster and the Royal Victoria Hospital, Belfast, UK.

11 September 2001
Electronics Letters Online No: 20010965
DOI: 10.1049/el:20010965

J.A. Santos, N.E. Evans and J.McC. Anderson (*N. Ireland Bioengineering Centre, School of Electrical and Mechanical Engineering, University of Ulster, Newtownabbey, Co Antrim, Northern Ireland, BT37 0QB, United Kingdom*)

G. Manoharan, B.J. Kidawi, J.D. Allen and A.A.J. Adgey (*Regional Medical Cardiology Centre, Royal Victoria Hospital, Grosvenor Road, Belfast, Northern Ireland, BT12 6BA, United Kingdom*)

References

1 BRONZINO, J.D.: 'The biomedical engineering handbook' (CRC Press & IEEE Press, 1995), 1275–1291
2 TIMMIS, A., and NATHAN, A.: 'Essentials of cardiology' (Blackwell Scientific Publications, 1993), 2nd Edn., 228–239
3 TOUBOUL, P.: 'Atrial defibrillator: is it needed? would society pay for it?', *Pacing Clin. Electrophysiol.*, 1995, **18**, (II), pp. 616–621
4 DONALDSON, P.E.K.: 'Frequency-hopping in r.f. energy-transfer links', *Electron. Wirel. World,* August 1986, pp. 24–26
5 DONALDSON, N., and PERKINS, T.A.: 'Analysis of resonant coupled coils in the design of radio frequency transcutaneous links', *Med. Biol. Eng. Comput.*, 1983, **21**, pp. 612–627

SC front-end with wide dynamic range

G.C.M. Meijer and V.P. Iordanov

A novel front-end circuit for capacitive sensors and switched-capacitor (SC) circuits is presented. In this circuit charge is transferred to an input integrator circuit in a controlled way to prevent overload of the input amplifier. Application of this technique extends the linear range for large input signals.

Introduction: Capacitive sensors are widely applied in cascade-sensor systems, in which a physical, chemical or mechanical quantity is converted into a capacitance value and further processed by an electronic circuit, the modifier. A simplified circuit of a typical front-end for such a modifier is shown in Fig. 1. In a sensor circuit the measurand can modulate the capacitor C_X or the voltage V_S. In both cases the measurand is transferred to a charge. At the instant t_0, this charge Q_X is transferred to the integrator. Next, integration of the (constant) reference current I_{REF} removes this charge. A comparator is monitoring the integrator output signal and actuates the switch control. At $t_0 + T$, the integrator output voltage crosses the threshold level it holds that:

$$Q_X + I_{REF}T = 0 \qquad (1)$$

where T is the time needed to remove the charge Q_X. By repeating this process periodically a charge-to-period converter is obtained. According to this simple principle many high-performance modifiers for sensor signals are made [1 – 4].

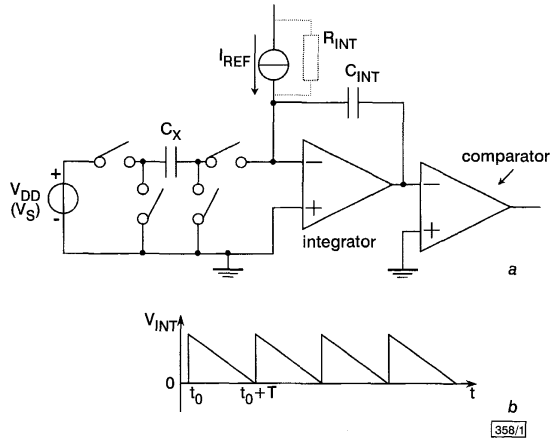

Fig. 1 *Simplified front-end circuit in the modifier and integrator output voltage against time*

a Front-end circuit
b Integrator output voltage against time

To reduce the effect of the comparator noise, the integrator output voltage should be large enough, which is achieved by selecting the capacitor value C_{INT} small enough. We have selected C_{INT} = 10 pF. In integrated smart sensors such a small capacitor value offers the additional advantage to occupy only a small chip area. However, with such a small value of C_{INT}, a problem arises when this front-end circuit is used with a large capacitor C_X or a large voltage V_S. When a large charge Q_X is transferred to the integrator at once, this will cause an overload of the applied amplifier. If the output is clipped, the open loop gain of the integrator operational amplifier decreases strongly. Then, the input signal of this amplifier is no longer negligible, and the reference current I_{REF} changes, caused by the source resistor R_{INT} not being infinite.

As can be concluded from eqn. 1 this causes nonlinearity in the charge-to-period conversion. An even worse nonlinearity can occur when input (protection) diodes are present. In the case of a large input voltage of the operational amplifier, these diodes can start to conduct. This will cause signal-charge loss at the integrator input. To extend the linear region, of the charge-to-period converter, without increasing the value the capacitor C_{INT}, a new front-end circuit has been designed.

New circuit: Fig. 2*a* shows the circuit diagram of the novel circuit. In this circuit, clipping of the amplifier output is avoided by using a negative feedback circuit, which controls the discharge of the capacitor C_X. The action of this feedback circuit can be explained by considering the integrator output voltage over a complete period (Fig. 2*b*).

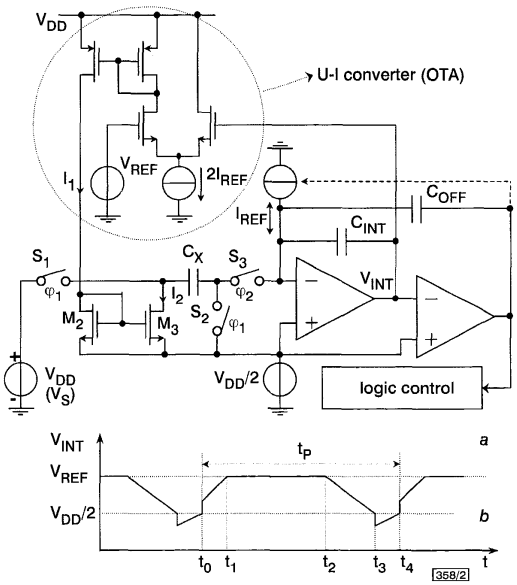

Fig. 2 *Proposed circuit diagram and integrator output voltage against time*

a Proposed circuit
b Integrator output voltage against time

During the time interval just in advance of t_0 the switches S_1 and S_2 are closed and the voltage source V_{DD} charges the capacitor C_X. Next, S_1 and S_2 are opened and S_3 is closed. Now the charge transfer to the integrator starts. This charge transfer is controlled by the output current I_2 of the current mirror (M_2 and M_3) in the following way:

During the time interval t_0^+ to t_1 the integrator output voltage is small. Consequently, it holds that $(I_2 = I_1) > I_{REF}$. The differential current $(I_2 - I_{REF})$ charges the integrator capacitor C_{INT}, which causes an increase of V_{INT}.

During the time interval t_1 to t_2 the output voltage V_{INT} is approximately equal to V_{REF}. The input stage of the U-I converter is in balance. This causes $I_1 = I_2 \simeq I_{REF}$. Because $(I_2 - I_{REF})$ is approximately zero, the integrator output voltage remains constant. However, the capacitor C_X is still discharged by the current I_2. This situation continues till the drain-source voltage of the MOS transistor is dropped so far that M_3 starts to be biased in the triode region.

During the time interval t_2 to t_3 M_3 is biased in the triode region. Consequently, the left-hand side of the capacitor C_X is connected to ground via the ON resistance R_{ON} of M_3. The small remaining charge in C_X is transferred to C_{INT}. In practical circumstances the time constant R_{ON} C_X appears to be negligible. Next, the capacitor C_{INT} is linearly discharged by the reference current I_{REF}.